Arabian Journal of Chemistry (2022) **15**, 104171

King Saud University

Arabian Journal of Chemistry

www.ksu.edu.sa
www.sciencedirect.com

ORIGINAL ARTICLE

Optimized adsorption and effective disposal of Congo red dye from wastewater: Hydrothermal fabrication of MgAl-LDH nanohydrotalcite-like materials

Mohamed A. Farghali [a],*, Abdelfattah M. Selim [b], Hanem F. Khater [c], Noha Bagato [d], Walaa Alharbi [e], Khadijah H. Alharbi [e], Ibrahim Taha Radwan [f]

[a] *Nanotechnology and Advanced Materials Central Laboratory (NAMCL), Regional Center for Food and Feed (RCFF), Agricultural Research Center (ARC), Giza, Egypt*
[b] *Department of Animal Medicine (Infectious Diseases), College of Veterinary Medicine, Benha University, Toukh 13736, Egypt*
[c] *Department of Parasitology, Faculty of Veterinary Medicine, Benha University, Toukh 13736, Egypt*
[d] *Egyptian Petroleum Research Institute (EPRI), PO Box 11727, Nasr City, Cairo, Egypt*
[e] *Department of Chemistry, College of Sciences & Arts, King Abdulaziz University, Rabigh, Saudi Arabia*
[f] *Supplementary General Sciences Department, Faculty of Oral and Dental Medicine, Future University in Egypt, Cairo 11835, Egypt*

Received 8 February 2022; accepted 4 August 2022
Available online 10 August 2022

KEYWORDS

Layered double hydroxide;
Adsorption;
Congo red;
Langmuir isotherm;
Pseudo-second-order kinetic

Abstract The effectiveness of Congo red (CR) adsorption from aqueous solutions onto MgAl-layered double hydroxide (MgAl-LDH) nanosorbents was examined in this study. MgAl-LDH was synthesized using the hydrothermal method, and physicochemical characterization was performed via powdered X-ray diffraction, high-resolution transmission electron microscopy, Fourier transform infrared analysis, and zeta potential measurements. For optimum adsorption of CR onto the synthesized MgAl-LDH nanosorbent, the adsorption process was employed in batch experiments. Adsorption parameters, such as the adsorbent dosage, solution pH, contact time, and initial adsorbate concentration, vary with the adsorption kinetics and isotherm mechanism. The results of the batch experiments indicated rapid adsorption of CR dye from aqueous solutions onto MgAl-LDH during the first 30 min until equilibrium was achieved at 180 min with

---

* Corresponding author.
E-mail addresses: mgoda199@gmail.com, mohamedfarghaly_p@sci.asu.edu.eg (M.A. Farghali), Abdelfattah.selim@fvtm.bu.edu.eg (A.M. Selim), hanem.salem@fvtm.bu.edu.eg (H.F. Khater), nohabagato@hotmail.com (N. Bagato), wnhalharbe@kau.edu.sa (W. Alharbi), khalharbe@kau.edu.sa (K.H. Alharbi), ibrahim80radwan@hotmail.com (I. Taha Radwan).

Peer review under responsibility of King Saud University.

ELSEVIER **Production and hosting by Elsevier**

https://doi.org/10.1016/j.arabjc.2022.104171

a dye concentration of 50 mg/100 mL and MgAl-LDH adsorbent dosage of 0.05 g. The experimental adsorption data fit adequately with the monolayer coverage under the Langmuir isotherm model ($R^2 = 0.9792$), and showed the best fit with the pseudo-second-order kinetic model ($R^2 = 0.996$). The change in zeta potential confirmed the effective adsorption interaction between the positively charged MgAl-LDH and the negatively charged CR molecules with electrostatic interactions. This work is distinguished by the successful hydrothermal preparation of MgAl-LDH in the form of homogenous nanoscale particles (~100 nm). The prepared MgAl-LDH showed a high adsorption capacity toward anionic CR dye with a maximum adsorption capacity of 769.23 mg/g. This capacity is higher than those reported for other adsorbents in previous research.

1. Introduction

A major source of industrial pollution is wastewater contaminated with organic dyes owing to their intensive use in several applicable industries, such as paper, textiles, printing, solar cells, plastics, and cosmetics (Wang, 2019; Zhu, 2022). The high toxicity, low biodegradability, and high chemical stability of these organic dyes cause serious problems when they are not disposed of properly (Zhang, 2016; Lan, 2022). In addition, the accumulation of these organic dyes in water streams has negative effects on human health and aquatic life due to their mutagenic and carcinogenic effects (Quan, 2019; Verma, 2022). Congo red (CR) is an anionic pollutant azo dye with a complex aromatic structure. It is non-biodegradable, highly soluble in water, and highly resistant to traditional degradation. Because it has carcinogenic properties, as well as being harmful to the skin, eyes, respiratory system, and reproductive system, it is very important to remove CR dye from wastewater before it can reach natural water bodies (Mittal, 2009; Liu, 2022; Arab et al., 2022). Different wastewater treatment techniques include ion exchange, photochemical degradation, precipitation, membrane filtration, electrochemical oxidation, ozonation, coagulation/flocculation, and biological treatment (Goddeti, 2020; Eltaweil, 2021; Madan, 2019). Adsorption technology is among the most important and simple techniques because it is inexpensive and has low energy consumption and high disposal efficiency (Raval, 2016; Hu, 2018). The effectiveness of the adsorption process depends on the nature of the sorbent. Thus, the choice of adsorbent is a vital factor in enhancing the adsorption process and its efficiency (Hu, 2018). The ideal adsorbent is efficient, low-cost, stable, and environmentally friendly (Zhang, 2018). In combination with adsorbent materials, the role of nanotechnology is to change the sorbent properties and morphology by increasing the adsorbent surface area, thus increasing the adsorption capacity and pollutant-removal efficiency (Madan, 2019). Clay comprising layered double hydroxides (LDHs) is anionic nature and expressed as $[M^{2+}_{1-x}M^{3+}_{x}(OH)_2]^{x+}[A^{n-}_{x/n}]^{x-}\cdot mH_2O$, where M^{2+}, M^{3+}, and A^{n-} indicate divalent metal cations, trivalent metal cations, and interlayer anions, respectively, and × represents the molar ratio of M^{3+} to the total metal, which ranges from 0.2 to 0.33 for pure LDH structures (Deng, 2018; Woo, 2011; Xie et al., 2021). Promising applications of LDH in the field of anion adsorption are attributed to the multilayer structure of LDH, which comprises positively charged layers with high surface area, high porosity, good interlayer anionic exchangeability, and low cost of production (Xie et al., 2021; Baliarsingh et al., 2013; Goh et al., 2008). Several types of LDHs have been prepared and applied as adsorbents to remove different contaminants from wastewater (Goh et al., 2008; Theiss, 2014; Jawad, 2019; Mittal, 2021). Herein, preparation, full characterization of MgAl-LDH nanohydrotalcite and studying the different parameters affecting the adsorption capacity of LDHs toward CR dye, such as the contact time, initial dye concentration, pH of the solution, and adsorbate.

2. Experimental work

2.1. Materials

Aluminum nitrate nonahydrate ($Al(NO_3)_3\cdot9H_2O$), magnesium nitrate hexahydrate ($Mg(NO_3)_2\cdot6H_2O$), sodium hydroxide (NaOH), CR dye ($C_{32}H_{22}N_6Na_2O_6S_2$), and decarbonated water were purchased from Alfa Aesar (Germany) and used without further purification.

2.2. Synthesis of MgAl-LDH

The salts of $Al(NO_3)_3\cdot9H_2O$ (0.5 M) and $Mg(NO_3)_2\cdot6H_2O$ (1.0 M) were mixed together at a Mg^{2+}:Al^{3+} ratio of 2:1, dissolved in 40 mL bidistilled water, and placed in a separatory funnel fixed in a one-gas inlet–outlet apparatus. A 2.0-M NaOH solution was prepared separately and placed in a three-neck round-bottom flask. Both the magnesium–aluminum and sodium hydroxide solutions were degassed by purging nitrogen gas. A salt solution of $Mg(NO_3)_2\cdot6H_2O$ and $Al(NO_3)_3\cdot9H_2O$ was added dropwise to the NaOH solution with vigorous stirring at 1500 rpm without heating for 6 h. The pH was held constant between 10 and 11 by adding 5 mL NaOH (2.0 M) every half hour. The white gelatinous precipitate of MgAl double-layer hydroxide was obtained through centrifugation at 12000 rpm at room temperature (25 °C) for 2 min and was perfectly washed several times with distilled water to eliminate any impurities. The white slurry was resuspended in 100 mL distilled water in a 250-mL Teflon–stainless reactor, heated for 14 h at 80 °C, and then separated by centrifugation. The slurry was dried at 70 °C for 48 h. The synthesis procedure for MgAl-LDH is depicted in Fig. 1.

2.3. Characterization of LDH nanoparticles

The morphology of the synthesized LDH was examined via high-resolution transmission electron microscopy

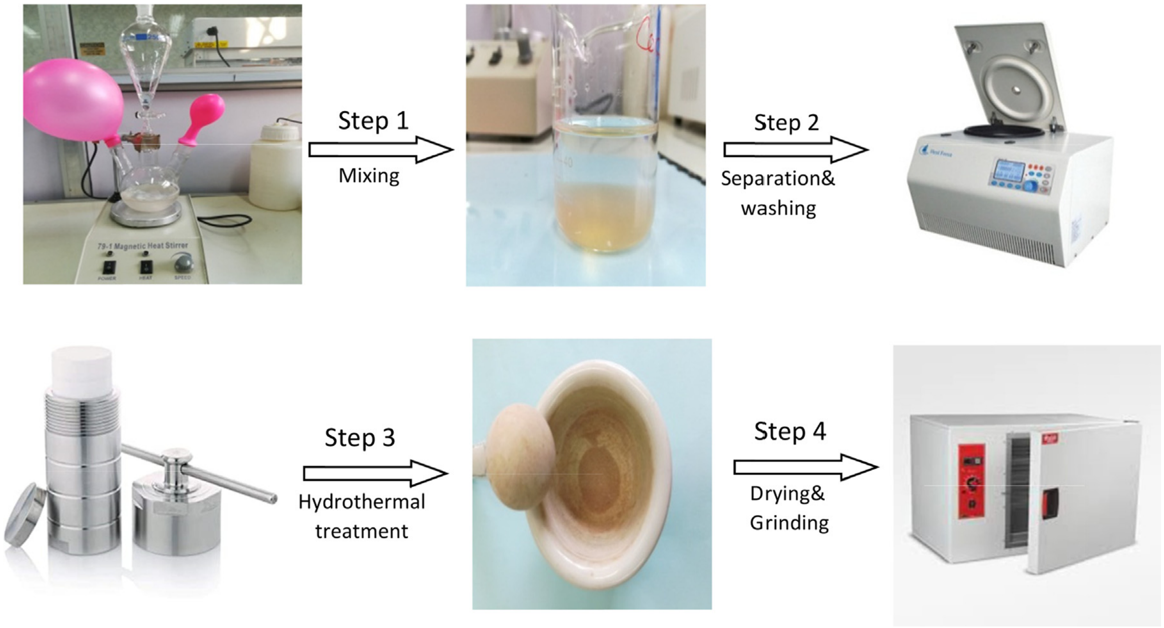

Fig. 1 Schematic procedure for the synthesis of MgAl-LDH.

(HR-TEM). The captured images were recorded with JEOL JEM-100 using an accelerating voltage of 200 kV. The powder X-ray diffraction (PXRD) patterns of LDH were obtained using X'Pert PRO Panalytical with Cu Kα radiation (λ = 1.5406 Å). The diffraction patterns were acquired as a value of 2θ in the scanning range of 4–80 with a scanning rate of 2.4°/min. The functional group and intact structure of the LDH were recognized by Fourier transform infrared spectroscopy (FT-IR, Frontier MIR/FIR spectrometer; Perkin Elmer) with a scanning range from 4000 to 400 cm^{-1} using the conventional dried KBr disc. The surface charge or zeta potential was inspected using a Zetasizer Nano ZS analyzer, where 1 mg of the powder was dispersed in 10 mL of distilled water.

2.4. *Adsorption study of Congo red*

CR adsorption to MgAl-LDH was performed at room temperature via batch experiment under varying adsorption conditions. For the adsorption kinetics and isotherm determination, the contact time ranged from 1 to 180 min, and 0.05 g of the sorbent was added to 100 mL of CR solutions with concentrations varying between 50 and 1000 mg/L and shaken using a benchtop shaker (Unimax 1010 DT; Heidolph, Germany; 350 rpm). The pH of the CR dye solution was also varied between 3 and 11 during the adsorption experiment, and the sorbent dose was changed from 0.01 to 0.2 g. The efficiency of the adsorption process was detected by measuring the color intensity of the remaining CR concentration using ultraviolet-visiblenear-infrared spectrophotometry (UV–vis-NIR; Cary 5000; Varian, UK) at λ^{max} = 498 nm of CR after preparing the calibration curve based on standard CR concentrations. The equilibrium adsorption capacity q_e (mg/g) was defined as the amount of adsorbed CR (mg) per unit mass of the sorbent (g) and can be determined by Equation (1) (Yan, 2017).

$$q_e = \frac{(C_0 - C_e)V}{m} \tag{1}$$

where C_0 and C_e are the initial and equilibrium CR dye concentrations (mg/L), respectively; m is the adsorbent mass (g); and V is the dye solution volume (L).

The removal efficiency percentage (R%) was obtained from Equation (2) (Jinhua, 2010).

$$\mathrm{R}\% = \left(\frac{C_0 - C_e}{C_0}\right) * 100\% \tag{2}$$

2.5. *Adsorption data analysis*

2.5.1. *Effect of contact time and kinetics study*

The kinetics study is required to express the adsorption rate of the contaminant (CR) on the surface of the sorbent (MgAl-LDH) to determine the residence time at the liquid–solid interface, determine the sorption mechanism, and determine the proper sorption treatment process (Qiu, 2009). Three adsorption kinetics models were employed to investigate the adsorption behavior: the pseudo-first-order, pseudo-second-order, and Elovich kinetic models. The correlation coefficients effectively describe the applicability of the corresponding kinetic models. The pseudo-first-order equation is (Simonin, 2016).

$$\ln(q_e - q_t) = \ln q_e - K_1 t \tag{3}$$

where q_t and q_e (mg/g) are the dye sorption capacity at time t (min) and at equilibrium, respectively; and K_1 (min^{-1}) is the pseudo-first-order reaction rate constant. The relation between ln ($q_e - q_t$) versus t yields a straight line with slope and intercept equal to K_1 and ln q_e, respectively.

The pseudo-second-order kinetic model is used to determine the adsorption of a single layer of solute (adsorbate) on a solid particle (adsorbent) without interactions between the sorbed species and is expressed as follows (Simonin, 2016; Faisal, 2021):

$$\frac{t}{q_t} = \frac{1}{K_2 q_e^2} + \left(\frac{1}{q_e}\right) t \tag{4}$$

where K_2 [g/mg·min] is the pseudo-second-order rate constant. The values of q_e and K_2 can be calculated from the slope and intercept of a plot of t/q_t versus t. In addition, h (mg/g·min) describes the initial sorption rate and is calculated according to Equation (5) (Ho et al., 2001).

$$h = kq_e^2 \tag{5}$$

The Elovich model equation is generally represented by (Wang et al., 2009).

$$q_t = \left(\frac{1}{\beta}\right) \ln(\alpha\beta) + \left(\frac{1}{\beta}\right) \ln t \tag{6}$$

where β is the desorption constant associated with the surface coverage extent and chemisorption activation energy (g/mg); and α is the initial adsorption rate (mg/g·min).

The straight line obtained from the relation between q_t and ln t provides the Elovich constants β and α from its slope and intercept, respectively.

2.5.2. Effect of initial adsorbate concentration and adsorption isotherms models

The experimental adsorption data are expressed mathematically using isotherm models to describe the relation between the initial concentration and adsorption capacity when the adsorbate is initially distributed at the equilibrium state between the solid and liquid phases. The adsorption capacity increases nonlinearly with increasing initial concentration (Zheng, 2009). Three adsorption isotherm models were used to fit the adsorption data, namely, the Langmuir, Freundlich, and Temkin isotherm models.

The Langmuir isotherm model can describe the monolayer coverage at specific homogeneous adsorbent sites without interaction between the chemical species adsorbed on the neighboring areas (Faisal, 2021; [32]). The simple form of the Langmuir isotherm model is represented as (Dehghani, 2016).

$$\frac{C_e}{q_e} = \frac{1}{bq_{\max}} + \left(\frac{1}{q_{\max}}\right) C_e \tag{7}$$

where C_e (mg/L) is the CR concentration at equilibrium; q_e and q_{max} (mg/g) are the equilibrium and maximum monolayer adsorption capacities, respectively; and b (L/mg) is the Langmuir constant associated with the adsorption energy, which describes the adsorbate's affinity toward the sorbent. The values of q_{max} and b can be calculated from the slope and intercept of the plot of C_e/q_e versus C_e, respectively. In addition, the value of the separation factor ($0 < R_L < 1$) of the Langmuir isotherm model denotes the feasibility of the adsorption process (Dehghani, 2016).

The Freundlich adsorption isotherm model is associated with the hypothesis that multilayer adsorption exists on heterogeneous adsorbent surfaces (Bharali and Deka, 2017), on which the active sites are not energetically uniform. The Freundlich model is expressed by Equation (8) (Yang, 2011).

$$\ln q_e = \ln k_f + \left(\frac{1}{n}\right) \ln C_e \tag{8}$$

where q_e (mg/g) is the equilibrium adsorption capacity; C_e (mg/L) is the concentration of CR at equilibrium; k_f (L/mg) is the Freundlich constant related to the adsorption capacity; and n (dimensionless) is a heterogeneity factor indicating the adsorption intensity. The value of n indicates the favorability of the adsorption process and has values within the range $0.1 < 1/n < 0.5$. Plotting ln q_e against ln C_e yields a straight line whose slope and intercept provide the values of n and k_f, respectively (Xie et al., 2021).

The Temkin isotherm model considers the presence of adsorbent–adsorbate interaction and assumes that the heat adsorption of all molecules in the layer decreases linearly with surface coverage. A linear decrease in adsorption energy as the adsorption sites are filled is also assumed, as well as a uniform distribution of binding energies up to a maximum value. The linear form for this model is (Lafi, 2016).

$$q_e = B \ln A_T + B \ln C_e \tag{9}$$

where q_e and C_e are the adsorption capacity (mg/g) and concentration (mg/L) of CR adsorbed species at equilibrium, respectively; B is related to the adsorption heat; and A_T is the Temkin isotherm binding constant at equilibrium and is associated with the maximum binding energy. Plotting q_e versus ln C_e enables the constants B and A_T to be obtained from the slope and intercept, respectively (Lafi, 2016).

$$B = \frac{RT}{b_T} \tag{10}$$

where R is the universal gas constant (8.314 J/kmol); T is the temperature (K); and $1/b_T$ (mol/J) is the adsorption potential of the adsorbent.

2.5.3. Effect of pH and sorbent dosage

The pH is a significant parameter reflecting the nature of the solid–liquid adsorption interaction and can affect the adsorbate's degree of ionization and the adsorbent's surface charge (Lafi, 2016). The effect of pH on the adsorption capacity of MgAl-LDH was investigated using CR solution with pH ranging from 3 to 11, adjusted by pH meter (Orion Versa Star; Thermo Scientific, USA) by dropwise addition of HCl (0.1 M) or NaOH (0.1 M).

The effect of the mass of MgAl-LDH on its adsorption of CR from aqueous solution was investigated using 100 mL of 500-mg/L CR solutions with the mass of sorbent varying from 0.01 to 0.2 g.

3. Results and discussion

3.1. Characterization of MgAl-LDH

The phase-determination results of free MgAl-LDH and MgAl-LDH intercalated with CR dye (MgAl-LDH-CR) are shown in Fig. 2. The PXRD diffraction patterns demonstrate that MgAl-LDH was perfectly synthesized with high crystallinity of the pure hydrotalcite phase, based on the presence of strong peaks located at $2\theta = 11.24°$, 22.68°, 34.34°, 38.19°, 45.17°, 60.30°, and 61.61° corresponding to reflection planes (*hkl*) of (003), (006), (012), (015), (018), (110), and (113), respectively, corresponding to the MgAl-LDH carbonate standard ICCD card (04–015–4253). The diffraction pattern of MgAl-LDH-CR after the adsorption process to show the peaks as free MgAl-LDH with multiple additional weak peaks is attributed to the presence of CR molecules intercalated to the MgAl-LDH surface. This indicates very good adsorption

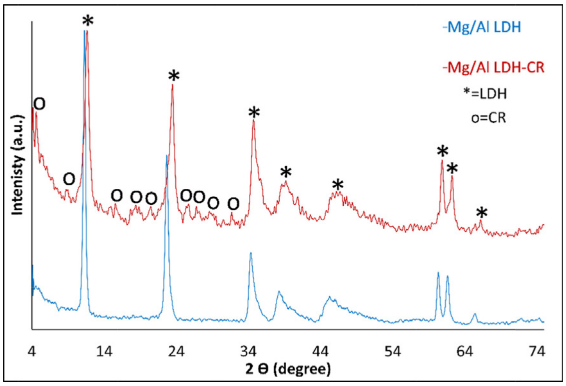

Fig. 2 PXRD Diffraction pattern of free MgAl-LDH and loaded LDH intercalated CR.

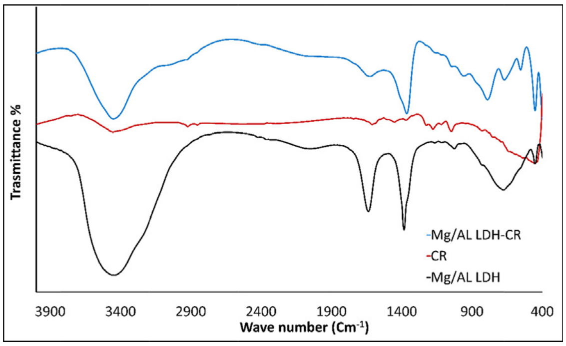

Fig. 3 FT-IR of free MgAl-LDH and loaded LDH intercalated CR and pure CR dye.

of CR via attachment to the layers and planes of the LDH. The peaks related to CR molecules are positioned at 2θ = 4. 54°, 15.55°, 18.36°, 20.45°, 25.66°, 26.83°, 28.55°, and 31.66°, corresponding to the CR reference card (00–036–1788). Furthermore, the diffraction pattern of CR-loaded MgAl-LDH exhibited peak broadening of the LDH crystal structure, which could be caused by the exchange of water molecules with CR molecules between the layers spacing of the LDH structure. This causes increased d-spacing of the LDH and, therefore, widens the peaks and decreases the crystal size of MgAl-LDH (Dasgupta, 2017). The FT-IR results, Fig. 3. are inconsistent with the PXRD results. In the case of the unloaded MgAl-LDH, a broadened band extended from 3300 to 3600 cm^{-1} that was attributed to the OH stretching vibration of water molecules present in the spacing between the LDH layers and metal hydroxides (Shabanian et al., 2020). A significant band approximately 1637 cm^{-1} is related to OH bending vibration. Other characteristic absorption bands are noted in the range of 450–1100 cm^{-1}, attributed to metal–oxygen and oxygen–metal–oxygen bands, including one at exactly 452 cm^{-1} due to the Al–O bond in $(AlO_6)^{-3}$ (Valcheva-Traykova et al., 1993). For MgAl-LDH-CR, all the absorption bands present in MgAl-LDH were also present, with the addition of bands related to the CR dye. A band related to the characteristic vibration stretching of the mono azo group (–N=N–) extended from 1500 to 1550 cm^{-1}. The peak at 1624 cm^{-1} is typical for red azo dyes. Furthermore, the weak bands at 1167 cm^{-1} and 1369 cm^{-1} are attributable to the asymmetrical stretching vibration of the S—O(SO_3–H) group and nitro group (NO_2). The morphological properties were examined using HR-TEM. According to Fig. 4A and 4B, the MgAl-LDH sorbent forms well-structured hexagonal nanostructures with sizes approximately 100 nm. In addition, the presence of the small bulky aggregations in MgAl-LDH-CR represented in Fig. 4B related to the accumulation of CR dye confirming the high absorptivity of LDH toward CR molecules on its surface, as well as the ion exchange of CR with the water molecules present between the LDH layers (Dasgupta, 2017). Zeta potential analysis was employed to characterize the surface charges of LDH at different pH values in the range between 3 and 13 to determine the point of zero charges (pH_{pzc}) value of MgAl-LDH, as shown in Fig. 5. It was clearly observed that the pH_{pzc} of MgAl-LDH is 12.0. At a pH lower than 12.0, the surface of the MgAl-LDH has positive charges, whereas at higher pH values, it has negative charges that can enhance the adsorption (Jia, 2019).

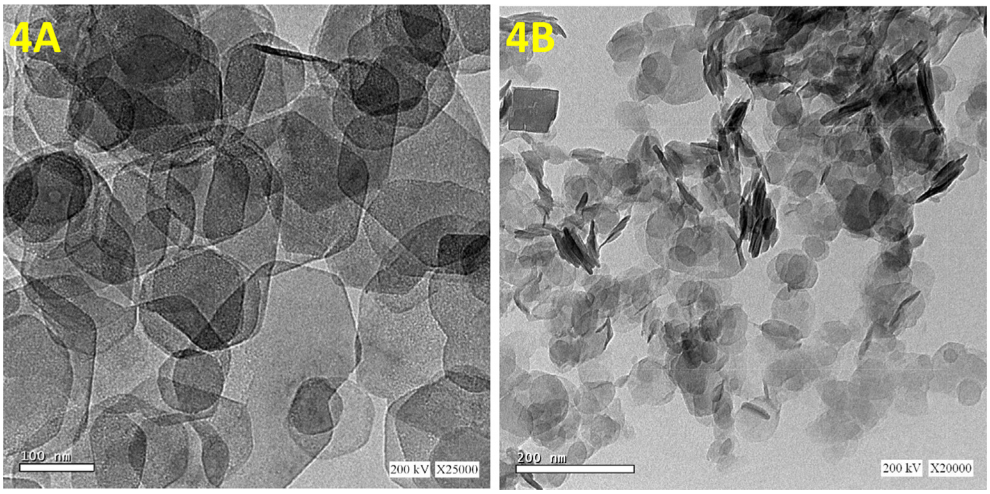

Fig. 4 HRTEM images of free MgAl-LDH (4A) and loaded LDH intercalated CR (4B).

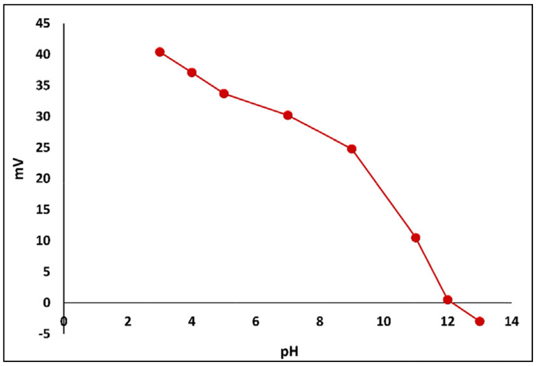

Fig. 5 Zeta potential measurements of the MgAl-LDH in aqueous solution with the variation of the pH values.

3.2. *Adsorption efficiency of MgAl-LDH*

3.2.1. *Effect of contact time and kinetics study*

The adsorption capacity of MgAl-LDH under varying contact time for the removal of CR is shown in Fig. 6A; the adsorption capacity increases with increasing reaction time, thus enhancing the removal of the CR contaminant from the aqueous solution until equilibrium is reached. The adsorption of CR was very fast in the first 30 min. After that, the adsorption gradually increases, indicating that the equilibrium state was reached after 180 min. The first stage is rapid due to surface complexation or electrostatic sorption onto the adsorbent. In contrast, weak sorption occurred in the second stage due to the insufficient free sorption active sites on the surface of MgAl-LDH (Ahmed, 2020).

The adsorption kinetics were studied by analyzing the experimental data with pseudo-first-order, pseudo-second-order, and Elovich kinetic models, as illustrated in Fig. 6B–6D. The kinetic parameters for adsorption of CR onto MgAl-LDH for the different kinetic models are listed in Table 1. Depending on the values of the calculated correlation coefficients (R^2), the pseudo-second-order model is much closer than the pseudo-first-order and Elovich kinetic models to describing the behavior of CR adsorption on MgAl-LDH (Taher, 2021). Furthermore, the values of the calculated equilibrium adsorption capacity (q_e) and the experimental adsorption capacity of the pseudo-second-order model are very close, which further proves the applicability of the pseudo-second-order model for predicting the adsorption process controlled by chemisorption (Sriram, 2020), in which the adsorption process is defined by electron exchange or sharing between the adsorbent and adsorbate (Miao, et al., 2021). Generally, LDHs possess a dual-charge nature, with positively charged brucite-like layers and negative interlayer anions, such as hydroxide ions. Consequently, the interaction between LDHs and CR is mainly dependent on the electrostatic interactions between the anionic CR and the positively charged LDH metal layers (Wang, 2018).

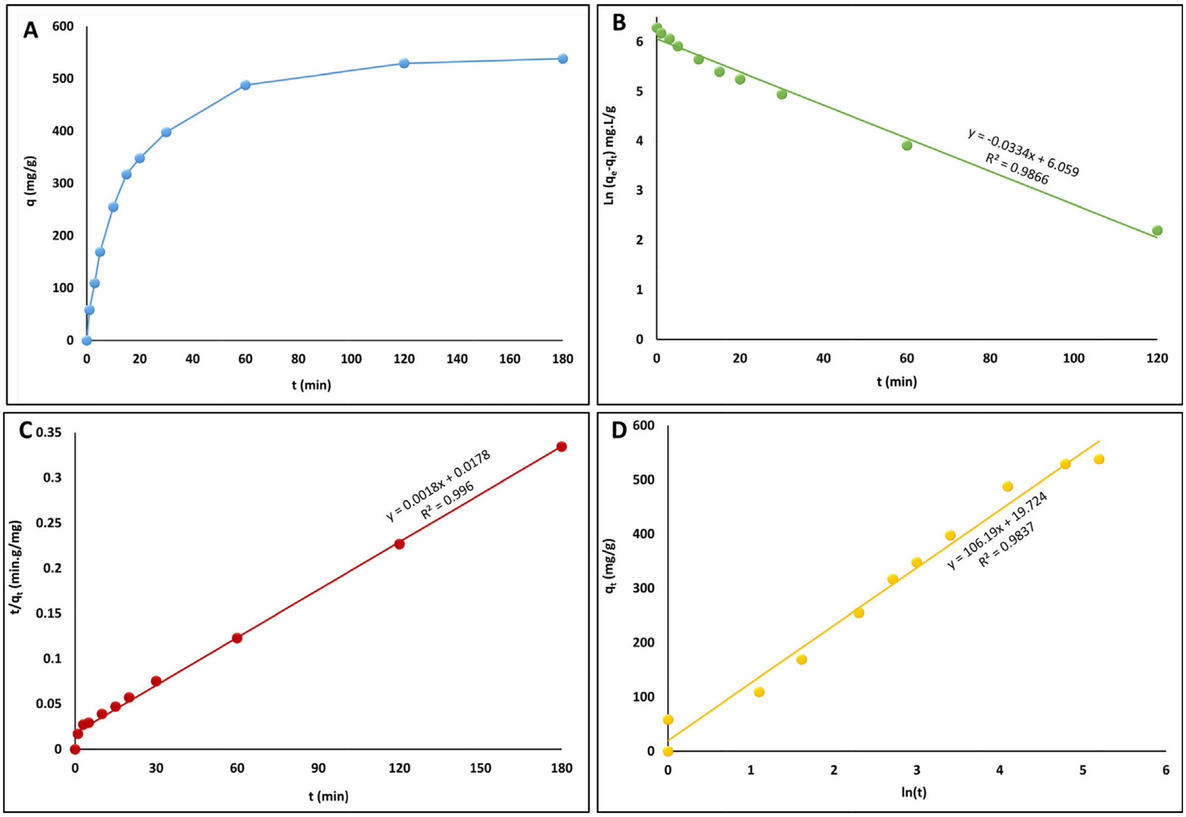

Fig. 6 Effect of contact time on the adsorption of CR onto MgAl–LDH (C_o = 500 mg/L, m = 0.05 g/100 mL) (A), and linear fitting adsorption experimental data of CR onto MgAl–LDH using pseudo-first-order (B), pseudo-second-order (C) and Elovich kinetic models (D).

Table 1 Kinetic parameters for adsorption of CR onto MgAl–LDH by different kinetic models.

Adsorbate	Pseudo-first-order model			Elovich model		
	q_{Calc} [mg/g]	K_1 [min^{-1}]	R^2	β [g/mg]	α [mg/g.min]	R^2
CR	427.95	0.0334	0.9866	0.0094	223.24	0.9837
Adsorbate	Pseudo-second-order model					
	K_2 [g/mg.min]	q_{Calc} [mg/g]		q_{Exp} [mg/g]	h [mg/g.min]	R^2
CR	0.00018	555.56		528.0	56.18	0.996

3.2.2. Effect of initial adsorbate concentration and adsorption isotherms models

The adsorption isotherms of MgAl-LDH were used to examine the relation between the adsorption capacity of the sorbent at different initial concentrations of adsorbate at room temperature that give important data for evaluating the adsorption system (Zhang, 2018). In Fig. 7A, it can be noted that with increasing initial concentration of CR solution, the adsorption capacity of MgAl-LDH increased sharply with a maximum adsorption capacity of 767.8 mg/g at 1000 mg/L CR. This phenomenon is attributed to the ratio between adsorbate species and the number of free active sites being small at low adsorbate concentrations, causing mass transfer resistance between the adsorbate aqueous solution and the adsorbent and leading to decreased adsorption capacity. In contrast, a higher initial concentration of adsorbate enhances the driving force beyond the mass transfer resistance of the adsorbate species, thus increasing the adsorption capacity of the sorbent (Aksu and Tezer, 2005; Farghali et al., 2021).

To further investigate the interaction between the adsorbate and adsorbent, the experimental adsorption data were analyzed using the Freundlich, Langmuir, and Temkin adsorption isotherm models, as shown in Fig. 7B–7D, and the calculated parameters are recorded in Table 2. The Freundlich model assumes that heterogeneous adsorption sites are present on the surface of the adsorbent, and that the adsorbed species mutually affect one another. In addition, adsorption in this model is not bound to the single layer (Zheng, 2018). However, the Langmuir model assumes that the adsorbed particles are mutually independent and tied in a single layer with the adsorbent surface. The Temkin model assumes that adsorbent–adsorbate interaction, and therefore the heat adsorption, decreases linearly with coverage for all molecules in the layer (Lafi, 2016). Compared with the Freundlich and Temkin mod-

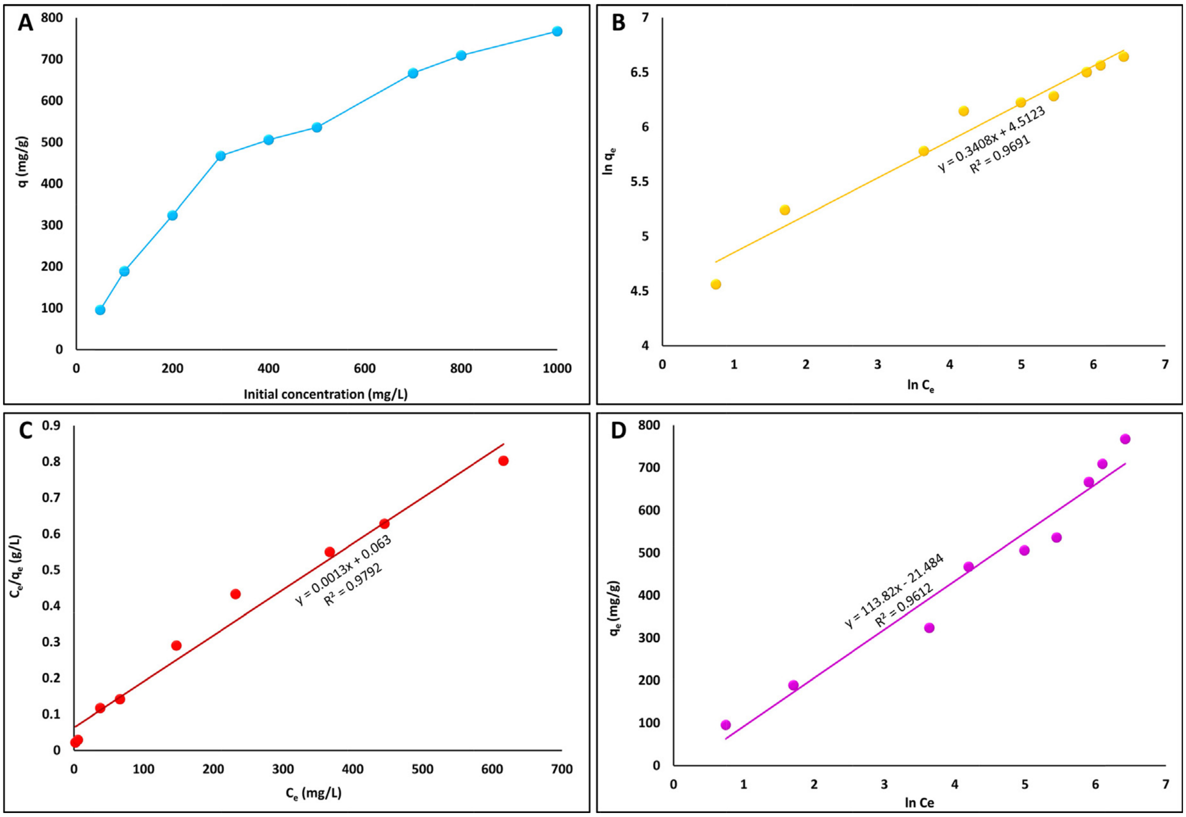

Fig. 7 Effect of initial CR concentrations (100–1000 mg/L) on adsorption capacity of MgAl–LDH for the removal of CR from aqueous solution (contact time = 120 min, m = 0.05 g/100 mL) (A), Linear fitting curves of the experimental adsorption data with the Freundlich isotherm model (B), Langmuir isotherm model (C) and Temkin isotherm model (D) for adsorptive removal of CR from aqueous solution using MgAl–LDH.

els, the Langmuir isotherm model showed the best fit for the experimental adsorption data of CR on MgAl-LDH with a correlation coefficient value ($R^2 = 0.9792$) greater than those of the Freundlich and Temkin models ($R^2 = 0.9691$ and 0.9612, respectively), indicating a monolayer adsorption process in which only a single layer of CR molecules can be adsorbed onto the surface of the MgAl-LDH sorbent. q_m of the MgAl-LDH is calculated from the Langmuir isotherm to be 769.23 mg/g, which is very close to the experimental value of 767.8 mg/g, providing further confirmation that the Langmuir isotherm model is a good fit for the adsorption data. According to Table 2, the calculated R_L values are within 0.046–0.492, indicating the favorability of the adsorption process. The lower value of the Langmuir constant (b) indicates CR's affinity toward MgAl-LDH.

Furthermore, the favorability of the adsorption process can be confirmed from the value of the Freundlich heterogeneity factor ($1/n$); in Table 2, $1/n = 0.34$ (Vimonses, 2009). A comparison of the previously recorded adsorption capacities of various sorbents for the removal of CR and that found in this work is listed in Table 3.

Table 3 Previously stated adsorption capacities of various sorbents for removal of CR in comparison with the current work.

Adsorbent	CR adsorption capacity, q_e [mg/g]	Reference
RGO/NH2-MIL-68(Al)	473.9	(Wu, 2017)
MNPs@NiFe LDH	79.6	(Taher, 2021)
Mesoporous activated carbon	14.2	(Mandal, 2021)
Micro-/nanostructured NiO microspheres	456.8	(Jia, 2021)
Mn-UiO-66@GO-NH2 composite	1265.8	(Eltaweil, 2021)
Hierarchical porous ZnO	334.0	(Lei, 2017)
Fe_3O_4@ZTB-1	458.0	(Han, 2019)
SBPF	417	(Zhang, 2016)
Gum ghatti acrylamide-grafted copolymer coated with zero-valent iron	153.3	(Goddeti, 2020)
Bentonite	158.7	(Lian et al., 2009)
ZnO@Ze composite	161.3	(Madan, 2019)
Chitosan/organo-montmorillonite	293.3	(Wang, 2007)
ZnO/SnO2 heteronanofibers	85.8	(Chen, 2015)
Powdered egg shell	96.0	(Zulfikar and Setiyanto, 2013)
MgAl-LDH	**769.23**	**[This work]**

3.2.3. *Effect of sorbent dosage and pH*

The amount of adsorbent added to the aqueous solution of contaminant significantly affects the removal efficiency of the adsorbate molecules during the adsorption process. Fig. 8. illustrates the effect of varying the amount of MgAl-LDH between 0.01 and 0.2 g/100 mL to remove CR from aqueous solution. A significant enhancement in CR removal from 14.8 % to 100.0 % is observed with increasing MgAl-LDH dose from 0.01 to 0.2 g/100 mL. The number of available adsorption active sites in aqueous solution increased with increasing adsorbent dose, thus increasing the probability of removing the contaminants from the aqueous solution. In contrast, the adsorption capacity of MgAl-LDH decreased with further increases in adsorbent dosage because the dispersion of adsorbent particles is uniform in aqueous solution for a specific adsorbent dosage range. All the available active sites are often entirely exposed, which enhances the accessibility of CR molecules onto a larger number of active sites. However, a further increase in adsorbent dosage leads to an increase in the number of adsorption active sites with higher energy, which could cause a decrease in a more significant fraction of active sites with lower energy, thus decreasing the adsorption capacity (Zubair, 2017). Photograph of the effect of MgAl-LDH dose on the adsorption capacity and removal efficiency of CR is shown in Fig. 9.

The pH is considered a significant factor affecting the adsorption process because of its influence on the surface functionalization of the solid adsorbent and the degree of ionization/dissociation of the adsorbate particles in the aqueous solution (Jia, 2019; Guan, 2017). The influence of pH on the adsorption capacity of MgAl-LDH to remove CR from aqueous solution is shown in Fig. 10. The results could be predicted from the behavior of the MgAl-LDH zeta potential curve in Fig. 5. The highest uptake of CR dye occurs when $pH < pH_{pzc}$, where $pH_{pzc} = 12.0$. This means that the surface of the adsorbent is protonated for $pH < 12$ due to the release of hydrogen ions, which can enhance the adsorption capacity of the adsorbent for anionic dyes through the generation of a strong electrostatic attraction force between the positively charged solid adsorbent surface and the negative charges of the negatively charged dye solution. In the MgAl-LDH interlayer, OH^-, HCO^{3-}, or CO_3^{2-} ions were substituted with the SO_3^- of the CR molecules via ion exchange (Li, 2016). With

Table 2 Adsorption isotherm parameters of MgAl–LDH for removal of CR from aqueous solution using Freundlich isotherm model, Langmuir isotherm model and Temkin isotherm model.

Adsorbate	Freundlich isotherm			Temkin isotherm			
	n	k_f	R^2	B	b_T [g/mol]	A_T [L/g]	R^2
CR	2.93	91.13	0.9691	113.82	21.77	0.828	0.9612
Adsorbate	Langmuir isotherm						
	q_{max} [mg/g]		B [L/mg]	R_L	R^2		
CR	769.23		0.0206	0.492–0.046	0.9792		

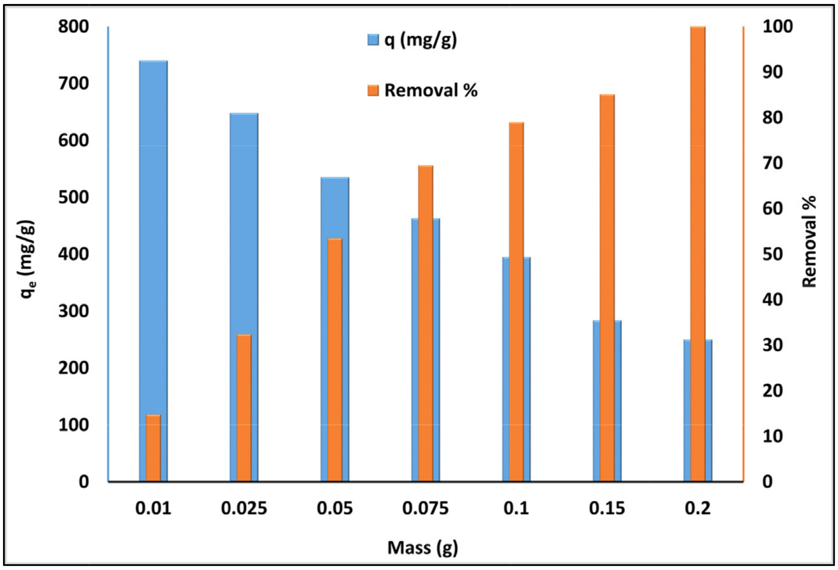

Fig. 8 Effect of MgAl–LDH dose on the adsorption capacity and removal efficiency of CR, (contact time = 120 min, C_o = 500 mg/L).

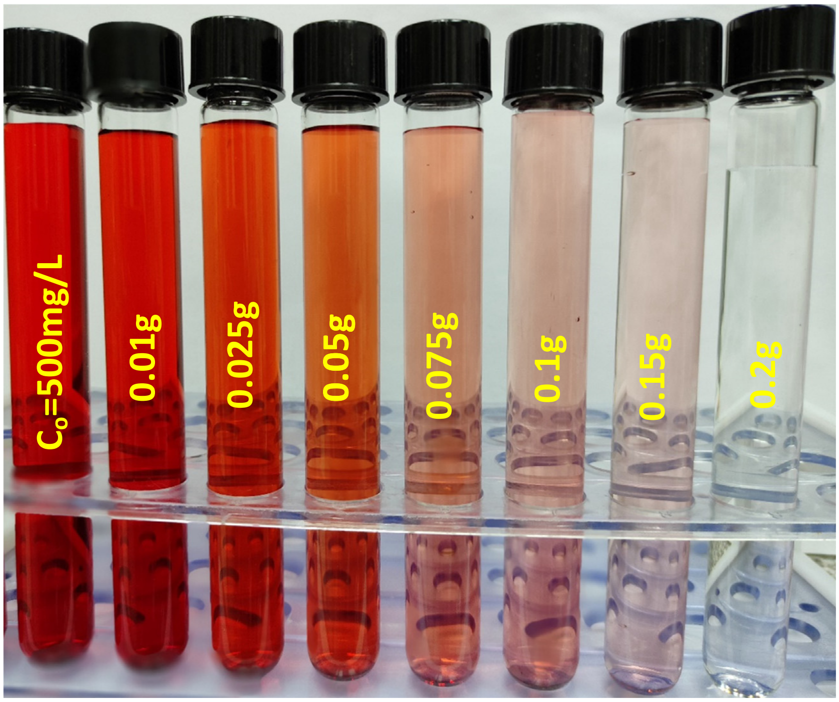

Fig. 9 Effect of MgAl–LDH dose photograph on CR's removal efficiency. (Contact time = 120 min, C_o = 500 mg/L, sorbent dose varying between 0.01 and 0.2 g/100 mL).

increasing pH of the CR solution, the positive charges on the surface of MgAl-LDH gradually decrease, and the negative charges increase; as a result, an acidic medium is needed to achieve the optimum adsorption conditions. As a consequence, the electrostatic attraction force between MgAl-LDH and the CR dye solution weakens gradually with increasing pH, resulting in a decrease in adsorption efficiency (Zheng, 2019). The effect of the solution pH photograph on CR adsorption by MgAl-LDH is presented in Fig. 11.

3.2.4. Adsorption mechanism

The adsorption mechanism of the CR anionic dye by MgAl-LDH nanosorbent comprises two mechanisms: adsorption on the external surface and ion exchange. In the first approach, the adsorption of CR occurs on the outer surface of sorbent through electrostatic attraction and H-bonding (Li, 2016). The electrostatic attraction generated between the negatively charged sulfonate group of CR dye and the positively charged LDH surface below the point of zero charges depends on the

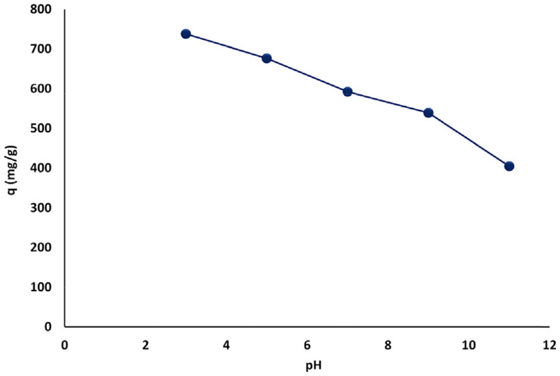

Fig. 10 Effect of solution pH on CR adsorption by MgAl-LDH nanosorbent (contact time = 120 min, C_o = 500 mg/L, m = 0.05 g, solution pH varying from 3 to 11).

Fig. 11 Effect of solution pH photograph on CR adsorption by MgAl-LDH (contact time = 120 min, C_o = 500 mg/L, m = 0.05 g, solution pH varying from 3 to 11).

value of the effectiveness of zero charges of MgAl-LDH, as shown in Fig. 5. H-bonding is favored between the hydroxyl groups of the LDH surface and negatively charged groups of CR dye (Chatterjee, 2007). The ion-exchange process entails inserting CR molecules and replacing the anions present in the interlayer spacing (CO_3^{2-}, HCO^{3-}, or OH^-) with CR anions (Lei, 2017; Olfs, 2009).

4. Conclusions

The sorbent was successfully prepared using a hydrothermal method, and its physicochemical properties were fully characterized via XRD, HR-TEM, FT-IR, and zeta potential analysis. It was then applied as an effective nanosorbent to remove anionic CR dye from aqueous solution. Different sorbent parameters, such as contact time, initial CR concentration, sorbent dosage, and pH, were studied as effective parameters in the adsorption of CR dye over the surface of the MgAl-LDH nanosorbent. The adsorption mechanism was enhanced by electrostatic attraction and H-bonding between the negative charges of the anionic CR dye and the positive surface of the MgAl-LDH nanosorbent below the point of zero charge. The results of the experimental data were fitted using the pseudo-second-order kinetic model and Langmuir isotherm model, which suggest a monolayer adsorption process with a maximum adsorption capacity of 769.23 mg/g, which is higher than that found in previous works using MgAl-LDH for the removal of CR.

Declaration of Competing Interest

The authors declare that they have no known competing financial interests or personal relationships that could have appeared to influence the work reported in this paper.

Acknowledgments

This work is partially funded by: This authors world like to thank the Science, Technology, and Innovation Funding Authority, Project title: “Eco-friendly Pesticides against Pests of Medical, Veterinary, and Agricultural Importance” ID: 41608 for partially supporting this study.

Funding

This work was partially supported by the Science, Technology, and Innovation Funding Authority, Project title: “Eco-friendly Pesticides against Pests of Medical, Veterinary, and Agricultural Importance” ID: 41608.

Appendix A. Supplementary material

Supplementary data to this article can be found online at https://doi.org/10.1016/j.arabjc.2022.104171.

References

Ahmed, D.N. et al, 2020. Waste foundry sand/MgFe-layered double hydroxides composite material for efficient removal of Congo red dye from aqueous solution. Scient. Rep. 10 (1), 1–12.

Aksu, Z., Tezer, S.J.P.B., 2005. Biosorption of reactive dyes on the green alga Chlorella vulgaris. Process Biochem. 40 (3–4), 1347–1361.

Arab, C., R. El Kurdi, and D. Patra, Zinc curcumin oxide nanoparticles for enhanced adsorption of Congo red: kinetics and adsorption isotherms study. 2022. **23**: p. 100701

Baliarsingh, N., K. Parida, and G.J.R.a. Pradhan, Influence of the nature and concentration of precursor metal ions in the brucite layer of LDHs for phosphate adsorption–a review. 2013. **3**(46): p. 23865-23878.

Bharali, D. and R.C.J.J.o.e.c.e. Deka, *Adsorptive removal of congo red from aqueous solution by sonochemically synthesized NiAl layered double hydroxide*. 2017. **5**(2): p. 2056-2067.

Chatterjee, S. et al, 2007. Adsorptive removal of congo red, a carcinogenic textile dye by chitosan hydrobeads: binding mechanism, equilibrium and kinetics. Colloids Surf. A: Phsicochem. Eng. Asp. 299 (1–3), 146–152.

Chen, X., et al., *The synthesis of ZnO/SnO 2 porous nanofibers for dye adsorption and degradation*. 2015. **44**(7): p. 3034-3042

Dasgupta, S., 2017. Controlled release of ibuprofen using Mg Al LDH nano carrier. IOP Conference Series: Materials Science and Engineering. IOP Publishing.

Dehghani, M.H. et al, 2016. Removal of chromium(VI) from aqueous solution using treated waste newspaper as a low-cost adsorbent: Kinetic modeling and isotherm studies. J. Mol. Liq. 215, 671–679.

Deng, L. et al, 2018. Sodium dodecyl sulfate intercalated and acrylamide anchored layered double hydroxides: a multifunctional adsorbent for highly efficient removal of Congo red. J. Colloid Interfaces Sci. 521, 172–182.

Eltaweil, A.S., et al., Ultra-high adsorption capacity and selective removal of Congo red over aminated graphene oxide modified Mn-doped UiO-66 MOF. 2021. **379**: p. 407-416

Faisal, A.A. et al, 2021. Green synthesis for novel sorbent of sand coated with (Ca/Al)-layered double hydroxide for the removal of toxic dye from aqueous environment. J. Environ. Chem. Eng. 9, (4) 105342.

Farghali, M.A., M.M. Abo-Aly, and T.A.J.I.C.C. Salaheldin, Modified mesoporous zeolite-A/reduced graphene oxide nanocomposite for dual removal of methylene blue and $Pb2+$ ions from wastewater. 2021. **126**: p. 108487

Goddeti, S.M.R. et al, 2020. Removal of Congo red from aqueous solution by adsorption using gum ghatti and acrylamide graft copolymer coated with zero valent iron. Int. J. Biol. Macromol. 149, 21–30.

Goh, K.-H., T.-T. Lim, and Z.J.W.r. Dong, *Application of layered double hydroxides for removal of oxyanions: a review*. 2008. **42**(6-7): p. 1343-1368.

Guan, T. et al, 2017. A facile approach to synthesize 3D flower-like hierarchical NiCo layered double hydroxide microspheres and their enhanced adsorption capability. Colloids Surf. A: Phsicochem. Eng. Asp. 529, 907–915.

Han, L.-J., et al., *Effective adsorption of Congo red by a MOF-based magnetic material*. 2019. **48**(14): p. 4650-4656

Ho, Y.S., J.C.Y. Ng, and G. McKay, *REMOVAL OF LEAD(II) FROM EFFLUENTS BY SORPTION ON PEAT USING SECOND-ORDER KINETICS*. 2001. **36**(2): p. 241-261.

Hu, M. et al, 2018. Ultra-high adsorption capacity of MgO/SiO2 composites with rough surfaces for Congo red removal from water. J. Colloid Interface Sci. 510, 111–117.

Jawad, A. et al, 2019. Selective removal of heavy metals by hydrotalcites as adsorbents in diverse wastewater: different intercalated anions with different mechanisms. J. Clean. Prod. 211, 1112–1126.

Jia, Y.-H., et al., Preparation of borate anions intercalated MgAl-LDHs microsphere and its calcinated product with superior adsorption performance for Congo red. 2019. **575**: p. 373-381

Jia, Y. et al, 2021. Fast removal of Congo red from aqueous solution by adsorption onto micro/nanostructured NiO microspheres. Mater. Sci. Eng.: B 270, 115228.

Jinhua, W. et al, 2010. Rapid adsorption of Cr (VI) on modified halloysite nanotubes. Desalination 259 (1), 22–28.

Lafi, R. et al, 2016. Adsorption study of Congo red dye from aqueous solution to Mg–Al–layered double hydroxide. Adv. Powder Technol. 27 (1), 232–237.

Lan, D. et al, 2022. Adsorptive removal of organic dyes via porous materials for wastewater treatment in recent decades: a review on species, mechanisms and perspectives. Chemosphere 293, 133464.

Langmuir, I.J.J.o.t.A.C.s., *The adsorption of gases on plane surfaces of glass, mica and platinum*. 1918. **40**(9): p. 1361-1403.

Lei, C. et al, 2017. Synthesis of hierarchical porous zinc oxide (ZnO) microspheres with highly efficient adsorption of Congo red. J. Colloid Interface Sci. 490, 242–251.

Lei, C. et al, 2017. Organic dye removal from aqueous solutions by hierarchical calcined Ni-Fe layered double hydroxide: Isotherm, kinetic and mechanism studies. J. Colloid Interface Sci. 496, 158–166.

Li, B., et al., Different dye removal mechanisms between monodispersed and uniform hexagonal thin plate-like MgAl–CO32–LDH and its calcined product in efficient removal of Congo red from water. 2016. **673**: p. 265-271

Lian, L., L. Guo, and C.J.J.o.h.m. Guo, *Adsorption of Congo red from aqueous solutions onto Ca-bentonite*. 2009. **161**(1): p. 126-131.

Liu, Y. et al, 2022. Fabrication of CoFe-MOF materials by different methods and adsorption properties for Congo red. J. Mol. Liq. 360, 119405.

Madan, S. et al, 2019. Adsorption dynamics of Congo red dye removal using ZnO functionalized high silica zeolitic particles. Appl. Surf. Sci. 487, 907–917.

Mandal, S., et al., Mesoporous activated carbon as a green adsorbent for the removal of heavy metals and Congo red: Characterization, adsorption kinetics, and isotherm studies. 2021. **243**: p. 103869

Miao, J., et al., *Feasible synthesis of hierarchical porous MgAl-borate LDHs functionalized Fe3O4@ SiO2 magnetic microspheres with excellent adsorption performance toward congo red and Cr (VI) pollutants*. 2021. **861**: p. 157974.

Mittal, A. et al, 2009. Adsorptive removal of hazardous anionic dye "Congo red" from wastewater using waste materials and recovery by desorption. J. Colloid Interface Sci. 340 (1), 16–26.

Mittal, J.J.J.o.E.M., Recent progress in the synthesis of Layered Double Hydroxides and their application for the adsorptive removal of dyes: A review. 2021. **295**: p. 113017.

Olfs, H.-W., et al., Comparison of different synthesis routes for Mg–Al layered double hydroxides (LDH): Characterization of the structural phases and anion exchange properties. 2009. **43**(3-4): p. 459-464

Qiu, H., et al., *Critical review in adsorption kinetic models*. 2009. **10**(5): p. 716-724

Quan, X. et al, 2019. Polyethyleneimine (PEI) incorporated Cu-BTC composites: Extended applications in ultra-high efficient removal of congo red. J. Solid State Chem. 270, 231–241.

Raval, N.P. et al, 2016. Adsorptive amputation of hazardous azo dye Congo red from wastewater: a critical review. Environ. Sci. Pollut. Res. 23 (15), 14810–14853.

Shabanian, M., Hajibeygi, M., Raeisi, A., 2020. FTIR characterization of layered double hydroxides and modified layered double hydroxides. In: Layered Double Hydroxide Polymer Nanocomposites. Elsevier, pp. 77–101.

Simonin, J.-P., 2016. On the comparison of pseudo-first order and pseudo-second order rate laws in the modeling of adsorption kinetics. Chem. Eng. J. 300, 254–263.

Sriram, G., et al., Mg–Al-layered double hydroxide (LDH) modified diatoms for highly efficient removal of Congo red from aqueous solution. 2020. **10**(7): p. 2285

Taher, T. et al, 2021. Preparation of magnetite-nanoparticle-decorated NiFe layered double hydroxide and its adsorption performance for congo red dye removal. Chem. Phys. Lett. 777, 138712.

Theiss, F.L. et al, 2014. A review of the removal of anions and oxyanions of the halogen elements from aqueous solution by layered double hydroxides. J. Colloid Interface Sci. 417, 356–368.

Valcheva-Traykova, M., N. Davidova, and A.J.J.o.m.s. Weiss, *Thermal decomposition of Mg, Al-hydrotalcite material*. 1993. **28**(8): p. 2157-2162.

M. Verma et al. Verma, M., et al., Multifunctional β-Cyclodextrin-EDTA-Chitosan polymer adsorbent synthesis for simultaneous removal of heavy metals and organic dyes from wastewater. 2022. **292**: p. 118447

Vimonses, V. et al, 2009. Kinetic study and equilibrium isotherm analysis of Congo Red adsorption by clay materials. Chem. Eng. J. 148 (2–3), 354–364.

Wang, L., et al., Removal of Congo red from aqueous solution using a chitosan/organo-montmorillonite nanocomposite. 2007. **82**(8): p. 711-720

Wang, X., et al., Cotton fiber-supported layered double hydroxides for the highly efficient adsorption of anionic organic pollutants in water. 2018. **42**(12): p. 9463-9471

Wang, Y. et al, 2019. In situ growth of ZIF-8 nanoparticles on chitosan to form the hybrid nanocomposites for high-efficiency removal of Congo Red. Int. J. Biol. Macromol. 137, 77–86.

Wang, X.S., Z.Z. Li, and S.R. Tao, *Removal of chromium (VI) from aqueous solution using walnut hull*. 2009. **90**(2): p. 721-729

Woo, M.A. et al, 2011. Phosphate-intercalated Ca–Fe-layered double hydroxides: crystal structure, bonding character, and release kinetics of phosphate. J. Solid State Chem. 184 (1), 171–176.

Wu, Z. et al, 2017. Highly efficient adsorption of Congo red in single and binary water with cationic dyes by reduced graphene oxide decorated NH2-MIL-68 (Al). J. Mol. Liq. 247, 215–229.

Xie, J., T. Yamaguchi, and J.-M.J.J.o.S.S.C. Oh, Synthesis of a mesoporous Mg–Al–mixed metal oxide with P123 template for effective removal of Congo red via aggregation-driven adsorption. 2021. **293**: p. 121758.

Xie, J., Yamaguchi, T., Oh, J.-M., 2021. Synthesis of a mesoporous Mg–Al–mixed metal oxide with P123 template for effective removal of Congo red via aggregation-driven adsorption. J. Solid State Chem. 293, 121758.

Yan, Y. et al, 2017. Flexible core-shell/bead-like alginate@PEI with exceptional adsorption capacity, recycling performance toward batch and column sorption of Cr(VI). Chem. Eng. J. 313, 475–486.

Yang, X. et al, 2011. Effect of pH, ionic strength and temperature on sorption of Pb (II) on NKF-6 zeolite studied by batch technique. Chem. Eng. J. 168 (1), 86–93.

Zhang, F. et al, 2016. Dual function magnetic hydroxyapatite nanopowder for removal of malachite green and Congo red from aqueous solution. Powder Technol. 302, 207–214.

Zhang, M. et al, 2016. Coal fly ash/CoFe 2 O 4 composites: a magnetic adsorbent for the removal of malachite green from aqueous solution. RSC Adv. 6 (96), 93564–93574.

Zhang, H. et al, 2018. Super adsorption capability of rhombic dodecahedral Ca-Al layered double oxides for Congo red removal. J. Alloy. Compd. 768, 572–581.

Zheng, H. et al, 2009. Sorption isotherm and kinetic modeling of aniline on Cr-bentonite. J. Hazard. Mater. 167 (1–3), 141–147.

Zheng, Y. et al, 2018. Fabrication of hierarchical bristle-grass-like NH4Al (OH) 2CO3@ Ni (OH) 2 core-shell structure and its enhanced Congo red adsorption performance. J. Alloy. Compd. 750, 644–654.

Zheng, Y. et al, 2019. 3D hierarchical graphene oxide-NiFe LDH composite with enhanced adsorption affinity to Congo red, methyl orange and Cr (VI) ions. J. Hazard. Mater. 369, 214–225.

Zhu, S. et al, 2022. Highly efficient and rapid purification of organic dye wastewater using lignin-derived hierarchical porous carbon. J. Colloid Interface Sci. 625, 158–168.

Zubair, M. et al, 2017. Recent progress in layered double hydroxides (LDH)-containing hybrids as adsorbents for water remediation. Appl. Clay Sci. 143, 279–292.

Zulfikar, M.A. and H.J.I.J.o.C.R. Setiyanto, *Adsorption of congo red from aqueous solution using powdered eggshell*. 2013. **5**(4): p. 1532-1540.